Numerical Modelling of Reinjection And Tracer Transport In A Shallow Aquifer, Nesjavellir Geothermal System, Iceland

Esteban Gomez-Diaz (e.gomez@geol.rwth-aachen.de)
RWTH Aachen University https://orcid.org/0000-0002-1209-8768
Samuel Scott
Reykjavik University
Thomas Ratouis
Carbfix, Bæjarháls 1
Juliet Newson
Reykjavik University

Research

Keywords: Numerical modelling, Geothermal reinjection, Dual porosity, MINC, Tracer injection, Fluid flow, Heat transfer.

Posted Date: October 20th, 2021

DOI: https://doi.org/10.21203/rs.3.rs-977658/v1

Numerical Modelling of Reinjection and Tracer Transport in a Shallow Aquifer, Nesjavellir Geothermal System, Iceland

Esteban Gómez-Diaz[1,2*], Samuel Scott[2,3], Thomas Ratouis[4], Juliet Newson[2]

[1]Energy and Minerals Resources Group, Geological Institute, RWTH Aachen University, Wüllnerstraße, 52056 Aachen, Germany.

[2]Iceland School of Energy, Reykjavik University, Menntavegur 1, 102 Reykjavik, Iceland.

[3] University of Iceland, Sæmundargata 2, 102 Reykjavik, Iceland.

[4] Carbfix, Bæjarháls 1, 110 Reykjavík, Iceland.

*Corresponding author: Esteban Gomez-Diaz e.gomez@geol.rwth-aachen.de

Abstract

Reinjection of excess water from the power production process in Nesjavellir geothermal field has increased the temperature of the shallow groundwaters, posing a risk to cold water wells used for the power plant as well as the ecosystem in Lake Thingvellir. Here, we present a numerical model of the fluid flow and heat transport in the re-injection zone to elucidate the flow path of reinjected liquid and the impact of reinjection on the temperature of groundwaters. The permeability model is based on a 3D geological model of the area and the numerical simulation is calibrated against underground water temperature data measured between 1998-2018 and also data from a tracer test data performed in 2018-2019. We find that the dual-porosity approach is necessary to reproduce the fast and high tracer returns measured in some wells. The model reproduces the overall

temperature field and shows how rift-parallel normal faults act as permeable channels controlling fluid transport. If injection continues, the temperature along the lava field increases considerably and spreads vertically to much deeper levels, generating a narrow warm zone along the main fault. If shallow injection ceases, the temperature drops rapidly at the surface, but around the reinjection zone temperatures decrease slowly and the subsurface temperature anomaly remains for the next 20 years. The numerical model in this study allowed a better characterization of the fracture matrix interface and the porosity of postglacial lava flows providing solutions for sustainable water management of the geothermal resource and the surrounding environment.

Keywords: Numerical modelling, Geothermal reinjection, Dual porosity, MINC, Tracer injection, Fluid flow, Heat transfer.

1. Introduction

Power generation from high-enthalpy geothermal systems requires the reinjection of significant quantities of hot water (40-80 ºC) remaining after the power generation process. The reinjection of this liquid in nearby wells can ensure the longevity of a geothermal resource by providing pressure support, improve heat recovery from the subsurface rock, and reduce the risk of subsidence, in addition to providing an environmentally friendly means of waste disposal (Stefansson, 1997; Axelsson, 2008; Axelsson, 2012; Kaya et al., 2011; Kamila et al., 2020). Depending on the depth and location of reinjection wells and overall fluid flow patterns, the negative effects of reinjection can be heating of shallow groundwaters, cooling of nearby production wells, and can trigger other undesirable effects such as ground subsidence (due to rock cooling and contraction) and induced seismicity (Diaz et al., 2016). Therefore, reinjection strategies must be carefully planned, and monitored.

Tracer testing is one of the primary ways to assess the impact of a fluid reinjection on surrounding groundwaters. The technique uses natural or induced variations in fluid chemistry or properties to obtain information about groundwater flow rates and directions, aquifer hydraulic and transport properties, and fluid–rock interaction (Axelsson, 2013; Maliva, 2016). In the geothermal context, tracer testing is used to assess the nature and properties of hydraulic connections, or flow-paths, between reinjection and production wells and to predict the rate of cooling of the production wells in response to long-term reinjection (Rose et al., 2010; Axelsson, 2013; Axelsson, 2012).

Results from tracer tests are commonly interpreted using analytical models that assume idealized one-dimensional flow channels connecting reinjection and production boreholes (Shook, 2005; Shook and Forsmann, 2005; Axelsson, 2013). Such models can simulate tracer return profiles quite accurately and yield estimates of the volumetric and hydraulic properties of the reservoir and flow channel. However, it is more challenging to match measured tracer returns with the three-dimensional numerical reservoir models more commonly used to investigate and optimize production and reinjection strategies for large-scale geothermal system management (O'Sullivan et al., 2016). While such models are commonly calibrated with measured downhole temperature and pressure data as well as production history data (enthalpy, mass flow rate, fluid pressure), tracer tests provide an additional source of data that can be used for model calibration, providing high resolution insight into the geometry and hydraulic properties of flow paths. Previous studies using tracer test data to calibrate three-dimensional geothermal reservoir models have shown that a dual-porosity approach is critical to reproduce the fast return profiles, and that good knowledge of the geometry of subsurface fractures is necessary in order to yield model

predictions that resemble the measured data (Pham et al., 2010; Buscarlet et al., 2015; Ciriaco et al., 2015; Ratouis., 2019).

In this study, we present a three-dimensional numerical simulation of shallow reinjection in the Nesjavellir geothermal field. The model is constrained by geological data, tracer tests conducted at the site from August 2018 to September 2019 and groundwater temperature data from 1998 until 2019. The aim of the research is to understand and characterize the fluid flow paths of reinjected water and forecast the impact of different reinjection strategies on thermal pollution of the nearby Lake Thingvellir and associated shallow groundwaters.

1.1. Nesjavellir Geothermal Power Station

The Nesjavellir Geothermal Power Station (NGPS) is located within the Hengill area of the Western Volcanic Zone in SW-Iceland, roughly 25 km east of Reykjavik (Fig. 1). The NGPS is the second-largest geothermal power station in the country, generating 120 MWe of electricity and 290 MWth of thermal energy for district heating. The power plant uses a combined cycle, wherein a steam is separated at 200 °C and 14 bars, and passed through four steam turbines, requiring 240 kg/s of steam in total. The steam is condensed in a tubular condenser and cooled to approximately 55 °C with cold groundwater, provided by a shallow fresh-water aquifer (Grámelur) in the lava field 6 km away from the power plant, directly to the S of Lake Thingvellir. The cooling water is heated in a heat exchanger to 87 °C by the ~190 °C hot geothermal water derived from the separators (Gíslason, 2000).

The excess water derived from the condensed steam and separated liquid is discharged either into shallow reinjection wells close to the power plant or into a nearby surface stream.. In both cases, warm water percolates underground and, therefore, increases groundwater

temperatures. Since the shallow discharge at Nesjavellir geothermal area started 23 years ago, there is evidence of thermal pollution of Lake Thingvellir, which is United Nation heritage site and a sensitive ecosystem with substantial populations of brown trout. In addition, increasing temperatures threaten the aquifer used for the cooling water. To understand and mitigate this problem, a monitoring campaign including tracer testing has been carried out to gain a better understanding of subsurface fluid flow paths. Along with geologic data, monitored temperature data and tracer test is used to calibrate the numerical model presented in this study.

1.2 Geologic background

The Nesjavellir geothermal field is situated in a rift valley extending from Hengill to Lake Thingvellir. The area is almost entirely built up of volcanic rocks of late Quaternary and postglacial age (Árnason et al., 1969), consisting mainly of hyaloclastite formations erupted during glacial periods and lava flows erupted during interglacial periods. Intrusions dominate at depths >1 km, and intermediate and felsic rocks are found at depth in many drill holes in the field (Franzson 1988; Franzson et al., 2010).

There are two major sets of normal faults in Nesjavellir associated ~10 km wide NE-SW-oriented graben structure that runs parallel to the hyaloclastite ridges (Franzson, 1988). One fault system is parallel to the NE-SW graben. The other system is oblique to the graben structure, with a strike of N-S that cuts through the valley (Franzson, 1988). These faults have an important role in controlling permeability within the geothermal system, as the N-S trending faults appear to act as partial barriers to northeastward flow along the NE-SW structures (Fig. 2a,c). The shallow groundwater aquifers are isolated from the deep geothermal system is isolated from the upper groundwater layers by a low permeability cap rock layer at ~0.5 km depth. Numerical calculations of shallow reinjection and tracer transport were performed with the TOUGH2 simulator and are

based on a geologic/conceptual model of the area. Here, we briefly describe the numerical methodology implemented in the TOUGH2 modelling focusing on the model set up as well as the tracer and temperature data used to calibrate the numerical model.

2. Methods

Numerical calculations of shallow reinjection and tracer transport were performed with the TOUGH2 simulator and are based on a geologic/conceptual model of the area. Here, we briefly describe the numerical methodology implemented in the TOUGH2 modelling focusing on the model set up as well as the tracer and temperature data used to calibrate the numerical model.

2.1. Conceptual model development

A three-dimensional geologic/conceptual model of the reinjection zone was developed using Leapfrog Geothermal 4.0 modelling software, see Fig. 3. The geologic model incorporates the surface geologic map by Hafstað et al. (2007) and borehole data from nine wells (NK-01, NK-02, NL-04, NL-07, NL-08, NL-09, NL-10, NL-11, NL-12) provided by Reykjavik Energy internal reports. The boundary to the bottom of the model was set to -0.5 km, corresponding to the depth of the deepest injection well NK-5. The bedrock lithology according this well is hyaloclastite, as is also observed in other shallow wells, such as NL-02, NL-10, NL-11, NL-07, NL-08 and NL-09. To the north, the geologic model is bounded by Lake Thingvellir. Hyaloclastite ridges determine the eastern and western model extents and location of the power plant defines the southern periphery. The high-temperature geothermal system, which is mainly located to the south of the power plant, is not included in this model as it is isolated from the shallow groundwater system by the cap rock.

The subsurface fault system in the Nesjavellir area were modeled based on the fluid pathways interpreted by the tracer test, field data and geological legacy information from a previous studys by Hafstað et al. (2007). The faults in the model are near-vertical, with a dip angle between 80-90°. The 3D geological/conceptual model of the shallow reinjection area of Nesjavellir geothermal field along with a cross-section cutting the vertical half of the model is illustrated on Fig. 3.

Injection of warm water takes place into deeper injection wells NN-01, NN-02, NN-03, NN-04, NN-05, NN-06, NN-07 and NN-09 and shallow injection wells less than 20 m which are SV3, LK and NS. The fluid is assumed to enter the system predominantly through the feedzones in each well. The depth of each feedzone for all the wells are shown in Table 1 and projected in Fig 3b.

Table 1. Location and depth of the feedzones in each reinjection well. Reinjected fluid is assumed to be evenly divided between each of the feedzones.

Well	Coordinates (x, y)	Feedzone depths (m)	Flow Ratio
NN-01	389994.59 402110.59	295	1
NN-02	390119.31 402298.09	415	1
NN-03	390105.09 402777.31	390, 445, 535	1/3
NN-04	390311.00 403200.31	280, 300, 330, 388	1/4
NN-05	390460.00 403090.00	220, 320, 520	1/3
NN-06	390450.00 403081.00	246, 280, 325, 425, 510	1/5
NN-07	390241.00 403242.00	200, 220, 255, 280, 400, 440	1/6
NN-09	389979.00 402471.00	310	1

2.2. Governing equations

The numerical simulations are performed in AUTOUGH2 (Croucher and O'Sullivan, 2000), a modified version of TOUGH2 (Pruess et al., 1999) developed by the University of Auckland TOUGH2 uses a fully implicit, integrated finite difference scheme to solve the governing

147 equations of mass and energy conservation. The basic mass and energy conservation equations can
148 be written as:

$$\frac{d}{dt}\int_{Vn} M^K dV_n = -\int_{An} \vec{F}^K \cdot d\vec{A}_n + \int_{Vn} q^K dV_n \qquad (1)$$

149 where integration is over an control volume V_n bounded by a closed surface A_n, n is a normal
150 vector on the surface element dA_n pointing inwards into V_n, M represents the mass or energy per
151 unit volume, with superscript $K = 1, \ldots,$ NK labeling the mass components (like water or dissolved
152 tracer) and $K = NK + 1$ the heat component, F denotes the mass or heat flux, and q denotes sinks
153 and sources. The last term expresses the fact that the rate of change of fluid mass in V_n is equal to
154 the net inflow across the surface of V_n plus net gain from the fluid sources. For the mass component
155 ($K = 1, \ldots,$ NK), the accumulation term is derived by summing over all the fluid phases for all the
156 components as given by the following equation:

$$M^K = \emptyset \sum_{\beta} S_\beta \rho_\beta X_\beta^k \qquad (2)$$

157 where the total mass of the component k is obtained by summing over the fluid phases β (liquid,
158 vapor), $\emptyset$ is the porosity, S_β is the saturation or volume fraction of the phase β (the fraction of pore
159 volume occupied by that phase), ρ_β is the density of phase β, and X_β^k is the mass fraction of
160 component k present in phase β. Heat accumulation is defined as the sum of the heat contained in
161 the rock and fluid given by:

$$M^{NK+1} = (1 - \emptyset)\rho_r C_r T + \emptyset \sum_{\beta} S_\beta \rho_\beta \mu_\beta^k \qquad (3)$$

162 where ρ_r and Cr are the density and specific heat of the rock, respectively, T is temperature and
163 μ_β^k is the specific internal energy in of mass component k in phase β. The advective flux of a mass
164 component k is given by:

$$F^K|_{adv} = \sum_{\beta} X_{\beta}^{k} F_{\beta} \quad (4)$$

with phase velocities calculated using Darcy's law:

$$F_{\beta} = \rho_{\beta}\mu_{\beta} = -K\frac{K_{r\beta}\rho_{\beta}}{\mu_{\beta}}(\nabla P_{\beta} - \rho_{\beta} g) \quad (5)$$

where k is the absolute permeability tensor, $k_{r\beta}$ is the relative permeability to phase β, μ_{β} is the kinematic viscosity, while P_{β} is the fluid pressure in phase β, ρ_{β} is density, and g is a vector of gravitational acceleration. Heat fluxes are controlled by conduction and convection, i.e.:

$$F^{NK+1} = -\lambda\nabla T + \sum_{\beta} h_{\beta} F_{\beta} \quad (6)$$

with λ as thermal conductivity and h_{β} is the specific enthalpy in phase β.

Fluid properties are calculated using equation-of-state module EOS1, which means fluid in the numerical model is assumed to be pure water with properties given by IAPWS-95 (Wagner and Pruß, 2002). The EOS1 module is suitable to simulate tracer transport with AUTOUGH2 (Yeh et al., 2012). The model was set-up as a dual-porosity model based on the Multiple Interacting Continua (MINC) approach Pruess and Narasimhan, 1982, 1985). The dual-porosity model of Nesjavellir used three interacting continua (one fracture and two matrix blocks) with corresponding volume fractions of 10% - 20% - 70% respectively and a fracture spacing of 100 m. The fracture was assigned a very high porosity fixed at 90%. The initial matrix porosity was chosen such that effective porosity of the dual-porosity model is the same as the porosity of the single porosity model. The MINC grid was applied only to the grid blocks within the central area limited by faults.

181 2.3. Model set-up

182 The model grid was set up using Leapfrog Geothermal and refined and optimized in the reinjection
183 area using PyTOUGH (Croucher, 2011). The thickness of the model is ~618 m, ranging between
184 119.69 masl. to -500 masl. with 19 layers of 45 meter thickness and two thinner near surface layers
185 of 5 and 20 meter thickness to represent the shallow flow better accurately. The model covers an
186 area of 50.2 km^2 and the groundwater table data defining the top surface was obtained from
187 Reykjavik Energy. The grid was rotated by 31° degrees to northeast with the purpose of orientating
188 the grid along an NNE direction parallel to the rift and some of the large NNE-SSW faults. The
189 alignment of the grid with the structure allows the model to use fault-parallel permeability higher
190 than the horizontal permeability perpendicular to the fault. The mesh consists of 22133 elements.
191 Visualization of the grid and model results were performed using Leapfrog and TIM (Yeh et al.,
192 2013), see Fig. 4.

193 Figure 5 shows the model geologic structure and the elevation of the groundwater table.
194 The hydrological parameters for the main rock types from the geologic model were based on
195 previous modeling studies of the Hengill area (Bodvarsson et al., 1990; Zakharova and Spichak,
196 2012; and Snæbjörnsdóttir et al., 2014; Gunnarsson & Aradóttir, 2014). Four rock types were
197 added as high permeability rocks to the conceptual model: CHN10, CHN20, CHN30 and FEED0.
198 The rock types CHN10, CHN20 and CHN30 correspond to permeability channels over the lava
199 field, as determined mainly by the recovery curve of the monitoring and trend of rise temperature
200 from field data. FEED0 represents permeable zone (layers 10 - 15 and 17) into the bedrock
201 determined by the feedzones. The bottom boundary is defined as the upper part of the layer that
202 limits the flow between the groundwater and the geothermal system (BOUN0). According to the
203 conceptual model and tracer test, the flow paths for the upper groundwater zone are confined to a

narrow SW-NE trending zone enclosed by lower permeability rocks on the NW and SE margins, and below around 50 m depth. These low permeability zones extend to the boundaries of the numerical model. The calibrated permeability values for the initial and added rock type are shown in Table 2.

Table 2 Calibrated permeability values for each rock type illustrated in figure 5.

ROCK TYPE	Permeability (m^2)		
	(kx)	(ky)	(kz)
GRA0	$1e10^{-09}$	$1e10^{-09}$	$1e10^{-11}$
GRU0	$1e10^{-14}$	$1e10^{-14}$	$1e10^{-15}$
HAG0	$1e10^{-09}$	$1e10^{-09}$	$1e10^{-15}$
NES0	$1e10^{-09}$	$1e10^{-09}$	$1e10^{-15}$
FAUH0	$1e10^{-16}$	$1e10^{-16}$	$1e10^{-16}$
FAU10	$3e10^{-11}$	$5e10^{-10}$	$5e10^{-13}$
FAU20	$3e10^{-12}$	$5e10^{-11}$	$5e10^{-13}$
FAU30	$3e10^{-12}$	$5e10^{-12}$	$5e10^{-13}$
BOUN0	$1e10^{-16}$	$1e10^{-16}$	$1e10^{-16}$
CHN10	$9e10^{-09}$	$9e10^{-09}$	$1e10^{-15}$
CHN20	$8e10^{-09}$	$8e10^{-09}$	$1e10^{-15}$
CHN30	$9e10^{-09}$	$9e10^{-09}$	$1e10^{-15}$
FEED0	$1e10^{-11}$	$1e10^{-11}$	$5e10^{-14}$
QDTP0	$1e10^{-16}$	$1e10^{-16}$	$5e10^{-16}$

Constant atmospheric conditions are applied over most of the top surface of the model, with a fixed pressure of 101325 Pa and temperature of 10 °C. For the columns lying under the lake (WETB0), a hydrostatic pressure corresponding to the depth of the lake and a constant temperature of 10 °C were assigned as a top boundary condition. The bathymetry of the lake was retrieved from (Stevenson et al., 2011).

2.4. Temperature and tracer test data

The temperature data used in the models were obtained from internal reports monitored by Reykjavik Energy and ISOR. The natural outflows temperature data relevant for this study for Lækjarhvar, Varmagjá, Sigguvík, Markagjá, Markatangi, Eldvík and Gramelur were monitored by

Reykjavik Energy since 1998 and were subsequently monitored by ISOR after 2000`s. They have measured temperature data from the monitoring stations in an annual record of the groundwater temperature in wells NK-1, NK-2, NL-2, NL-3, NL-4, NL-7, NL-8, NL-9, NL-10, NL-11 and NL-12.

The tracer tests used to calibrate the simulation model involved the injection of 2,7-NDS (Naphthalenedisulfonic acid disodium salt) in well NN-6 from November 2018 to September 2019. The average rate for the injection was 115 l/s for and 100 kg of tracer mass was injected. After 30 days of the injection, recovery was detected in NK-1, NK-2, NL-4, and NL-12 wells, with the largest concentration peaks detected in NK-1 and NK-2. There is a second recovery between 70 - 80 days for the natural outflows and NL-2 and possibly a third arrival after 150 days. The location of injection wells and monitoring points and, tracer recovery is illustrated in Figure 6, where the recovery data will be used to calibrate the simulation model.`

As the tracer is injected in relatively shallow groundwaters and not the deeper geothermal reservoir, it is assumed a neglected molecular diffusion, no phase changes occur in the flow channel and the mass of the tracer is conserved. Thermal degradation and chemical reaction with fluids and rocks in the reservoir does not occur and the density of the fluid within of the flow channel is nearly constant. Nevertheless, not all the injected tracer is recovered, most likely because some of the tracer is adsorbed in the rock matrix or flows outside the main flow-paths identified in this study.

The injection history from all shallow reinjection wells in the Nesjavellir area is incorporated in the model, since it is the total amount of injected and produced fluid that drives

240 the flow in the system. The injection and the discharge rates over the simulation time as well as
241 the temperature of the discharge water is shown in Figure 7.

242 Model manual calibration was carried out in order to obtain a return profile that shows
243 acceptable agreement with the measured tracer and temperature data. Although the models
244 simulate the system over different time periods, calibration of the tracer and temperature data was
245 performed jointly as both models are sensitive to the geologic structure and rock properties (mainly
246 permeability). The temperature simulation considers single water component from the 1st of
247 January 1998 until 5th of November 2018. This model uses the initial conditions described above
248 as well as the injection and production data for all wells along with the reinterpretation of the
249 structures based on the tracer recovery test from 2018 to 2019. The tracer calibration consists in a
250 two-component simulation that simulates the tracer injection with the second component
251 representing in the traces into appropriate model wells. The model simulates tracer advection from
252 the 15th of November 2018 until midnight on the 20th of September 2019. Geothermal fluid
253 injection and monitoring wells continues in the other wells in the system during this simulation.
254 In order to keep the steady tracer background value constant and prevent heavy dilution in all
255 injection elements, a miniscule amount of tracer ($1x10^{-10}$ kg tracer per kg injected water) were co-
256 injected within of the injections wells NN-01, NN-02, NN-03, NN-04, NN-06, NN-07, NN-09 and
257 surface injection point Lk during the simulation.

258 The calibrated model was used to forecast the temperature evolution in response to two
259 end-member scenarios: i) continued long term reinjection with average values of mass and ii)
260 immediate cessation of the shallow injection. The second scenario considers the amount of time to
261 achieve a steady-state after stopping all the reinjection and production activity in the shallow
262 groundwater field.

263 **4. Results**

264 4.1. Temperature model

265 The simulation shows a reasonably close match with the monitoring well temperature data over
266 the time, reproducing the overall rate and magnitude of temperature increase. The best matches
267 were obtained for NK-01, NK-02, NL-10, and NL-04 (Fig. 8). Seasonal fluctuations on the order
268 of ~10 C result from the variable injection of hot water (changing mass or changing temperature)
269 during the different time periods. Modest results were seen for wells NL-02, NL-07, NL-08 and
270 NL-09, whereas NL-11 showed temperature significantly lower than field data.

271 The measured temperature increase in natural outflows is less than the shallow monitoring
272 wells (Fig. 9). Eldvík reproduce the seasonal affect, although with a lesser amplitude than
273 measured (Fig. 9a), Markagjá simulation has a slight increase in the beginning of the 2000s, overall
274 results produce a lower temperature than measured (in the order of 5°C). Although data suggest
275 the greatest temperature increase in Varmagjá, the models predict a similar magnitude of
276 temperature response as the other natural outflows, resulting in a 10-13 °C discrepancy between
277 the model and the field data.

278 In addition to the above temperature transients the measured temperature for depth profiles
279 were used to calibrate the model. While the model reproduces the temperature evolution in the
280 near surface (>1m depth) fairly well, there is some discrepancy between model results and in
281 monitoring well with depth field data. Figure 10 shows the temperature-depth profiles for NL-10
282 (top panel) and NL-12 (bottom) at four different times between 2001 and 2017. The simulations
283 reproduce the temperature gradient in NL-10 (Fig. 10 a-d) but do not reproduce the temperature
284 increase which is measured below some in the well. The simulations also predict such a sharper
285 temperature inversion in NL-12 (Fig. 10e-f) the deepest monitoring station. However, the field

data indicate a warm plume between 60 m to 160 m depth that first increases and then decreases in magnitude over the simulation period which is not matched in the model. Other stations such as NK-01, NK-02, NL-04 and NL-07 showed measurements over restricted depths (<5 m) but reasonable matches through 20 years, with a slight difference and discrepancy on certain dates.

Heat transport is controlled by the presence of shallow high permeability aquifers in the near surface as well as major rift-parallel faults, which transport heat advectively from reinjection to the NW along the rift. Figures 11-13 compares the temperature distribution in the lava field at ~100 masl. (layer 1) with isotherms performed by ISOR for September 2000, October 2006 and May 2017. Soon after the beginning of shallow reinjection (Fig. 11), a plume with temperatures 20-40 C develops approximately centered along the most permeable fault (FAU10). Temperatures along this fault show that temperature is elevated only in the uppermost, high permeability, lava flows. Temperature remains unchanged at greater depths since the injection of warm water at deep levels has not yet started. The simulation illustrates that temperature increases most rapidly in the NE-SW, reaching 30 °C in the center of the field and 15-20 °C close to the lake, a good overall match to the field data. In addition, the simulations reproduce the bending of the thermal plume towards the east along the shore of Lake Thingvellir.

By October 2006 (Fig. 12), temperature increases to ~20 °C throughout most of the lava field with the area between 20 °C and 30 °C isotherms extending to the lake. At depths 0 - 0.5 km, temperature has increased to 60 °C close to the deep injection wells (NN-3, NN-4 and NN-5), but extends a smaller distance to the NW compared to temperatures in the shallow lava flow. The simulation shows a low temperature area (15 °C) between NK-02 and NL-11 as is expected due to this area is no under high permeability zone known since there is absence of geological and

308 monitoring data confirm that. As result, the warm flow is not significantly interacting in mentioned
309 area for this model.

310 By May 2017 (Fig. 13), temperature has increased to ~35 °C in the center of the area,
311 especially along the injection well to NK-02 and along the edge of the lake. However, the
312 temperature has increased over a significant area of the lava field, mainly with a northeast trend
313 seen in the field data as well as simulation results. At deeper levels temperature has increased
314 significantly, even rising to a shallow level below the NK-01 and KN-02. The temperature is
315 around 30-40 °C over a large vertical interval in the subsurface and extends ~3-4 km to the NW
316 along the main rift-parallel fault. The bend in the thermal plume to the west in the vicinity of Lake
317 Thingvellir is clearly visible, although the model predicts somewhat high temperatures (~20 C)
318 extend 1 km to the SW.

319 Overall, modeled temperatures correspond well with measured temperatures. Figure 14
320 compares a temperature model made in Leapfrog based on data collected in 2018-2019 with model
321 predictions. The broad zone with temperature (>50 C) around the deep injection wells in the SE
322 (cross-section A-A', Fig. 14b). To the NW (cross-section B-B', Fig. 14c), elevated temperatures
323 become increasingly confined to the depths <0.1, and the highest temperatures are focused on the
324 center along the main permeable fault. The simulations predict a more extensive area of elevated
325 temperature spread out to the southeast in the near vicinity of the lake (Fig. 14d).

326 4.2. Tracer approach

327 Tracer advection is controlled by the shallow high permeability lava flow at shallow depths and
328 the SW-NE oriented fault at greater depth. Model results show reasonable agreement with the field
329 data collected during the tracer test in 2018-2019. Figure 15 shows the tracer distribution at 86
330 masl. (Fig. 15a-d) and -180 masl.(Fig. 15e-g). A relatively broad (~0.5 km) plume of tracer is

found within the shallow lava flow. This plume moves to the NW, and after 42 days has reached the shore of Lake Thingvellir. After 126 days, the highest tracer concentrations in shallow lava flow are confined to the area in the near vicinity of the lake. At greater depths (Fig. 15e-g), tracer concentrations are significantly elevated along the main NW-SE-oriented fault. While tracer mass is greater at depth within the fault compared to the shallow lava flow, the anomaly is not as broad.

The simulations reproduce the overall arrival time, peak tracer concentration and shape of the measured tracer return curves in several of the monitoring stations, particularly NK-01 and NK-02 (Fig. 16a,b). The field data record a more rapid tracer return in the natural outflows Varmagjá, Eldvík and Markagjá compared to the simulations (Fig. 16c-e). In the wells NL-02 and NL-04 the modeled and measured tracer concentration peak is similar, but the simulations suggest a relatively broad peak compared to the narrow peak measured in the field data (Fig. 16f,g). The simulations predict no tracer arrival in NL-12 , although very low concentrations were measured (Fig. 16g).

4.3. Future scenarios

Two different future scenarios were evaluated using the calibrated model. In the first case, the injection continues for 20 years with the same injection rate and temperature as during the period 2018-2019 (Fig 17). In the second , all shallow and deep reinjection is stopped across the field (Fig 18). After 10 years of reinjection, temperature at 86 masl (near the surface) increases slightly close to the edge of the lake but more strongly at depth along the main fault, with temperature increases up to 45 °C and 60 °C at 86 masl and -180 masl, respectively. After 20 years, most of the shallow lava field has temperatures >25 °C, with values close to 35-40 °C in the main channels and 30 °C close to the lake. At 86 masl. the maximum temperature is around 60 °C, with temperatures around 50 °C in the main channel and 40 °C in the Grámelur area. At depths of -180 masl., the zone of

354 elevated temperature (60 °C) reaches the shoreline. The vertical cross sections along the most
355 permeable fault highlight the increasing temperatures with time.

356 In the case 2 (Fig. 18), the injection and production in the field were stopped. The
357 temperature drops drastically on the surface after less than two years, and a little more slowly at
358 depth. After 10 years, the shallow temperature is 12-13 °C, close to the initial temperature prior to
359 the beginning of reinjection. At greater depths, temperatures >30 °C persist in the area surrounding
360 the injection zone and along the main channel, but the area closer to the lake cools rapidly.

361

362 **5. Discussion**

363 The results from this modeling study show that the transport of heat and fluid in the Nesjavellir
364 reinjection zone is controlled by the heterogeneous permeability structure. At shallow depths (<0.1
365 km), reinjected fluid spreads out within a high permeability lava flow that extends to the shores of
366 Lake Thingvellir. Fluid reinjected at greater depths is controlled mainly by a rift-parallel normal
367 fault that channels the fluid towards the northwest.

368 The simulations illustrate that fault zones act as flow paths that quickly channel the fluid
369 from the injection zone to the monitoring stations NK-01 and NK-02. The flow paths are controlled
370 by interconnected fractures that focus the fluid flow through the rock. At depths between -100 and
371 -400 masl, the injected hot fluid flows mainly through a vertically-oriented fault damage zone.
372 Other lithologies that bound this fault zone are not zones of large scale flow. The high temperature
373 rise in the rock matrix above the direct path between the two wells suggests that the flow was
374 concentrated in a narrow path between the injection and the monitoring wells as seen in the tracer
375 test.

In general, the models reproduce the temperature changes over between 1998 to 2018. Some mismatch may result from seasonal effects that are not captured in the models. In addition, the simulation did not consider smaller-scale permeability heterogeneities that may affect some fluid flow dynamics. The tracer test data strongly suggest the presence of a flow channel, corresponding to the NNE trending rift-paralle normal faults, that mainly connecting the wells NK-01, NK-02 and, Varmagjá, Eldvík and Markajía springs with the injection well NN-06. While the model results are an acceptable match between the simulated tracer return curve using a dual-porosity model and the actual tracer return profile for NK-01 and NK-02, the models do not as closely reproduce the tracer recovery curves at natural outflows. Further refinement of permeability structure in the vicinity of the outflows is needed to improve the match for the outflow springs.

Use of a dual porosity, Multiple Interacting Continua (MINC) proposed by Pruess, (1992) approach to enhance the resolution of spatial discretization in the narrow flow channel showed clearly better results than single porosity, as would be expected for fracture-dominated permeability such as Nesjavellir. MINC approach reduces the effective volume of the block that the fluid flows through (fractures), causing the tracer travel time between the injection well and the production wells to be significantly faster.

The simulation shows if the injection continues for 20 years more with the average flow mass used during the period 2018-2020, the temperature at one meter below the groundwater table in the most lava area will be over 25 °C, increasing to over 35 °C at -90 masl., reaching to 50 °C for areas below the permeable channel and around it. Below the edge of the lake the deep temperature (-180 masl.) will increase around 50 °C. In the case if all injection and production activity ceases, the temperature will decrease rapidly on the surface, reaching values close to the

399 initial conditions in less than 2 year and after 10 years will almost as the initial conditions for the
400 top surface. However, given the temperature rise by injection in recent years, the cooling process
401 will take a little longer for deep levels.

402 Quality of data is essential to create and calibrate a numerical simulation model. The
403 availability of geological data used to build the Leapfrog model and constrain the permeability
404 structure was limited. In addition, there is limited data for deep temperatures. The temperature
405 inversion below 50 masl. predicted by the simulations is not seen in the deepest monitoring well,
406 NL-12, where simulation shows a good approximation over time in the bottom of the well but not
407 at intermediate layers. However, the others monitoring stations show reasonable results.

408 For further studies, an additional monitoring station between NL-11 and NK-02 may be
409 useful to understand the fluid flow between those wells and, measurements at depth levels of NK-
410 1 and NK-02 also could be a great tool for more accurate forecasting. Further refinement of
411 permeability values is needed to improve the match time recovery for springs. Additionally, seven
412 other tracers were injected in the system during the tracer test in 2018-2019. Calibrating the models
413 for each tracer as was done in this study would improve the understanding of the flow path,
414 especially the part near the lake over the lava Nesjahraun that was not possible to characterize very
415 well with the data presented here. The numerical dispersion results from the solution of the
416 advection equation is a function of grid block size and time step size. Therefore, further refinement
417 the grid could help increase the permeability and thus improve the numerical model. In addition,
418 revisited bottom boundary conditions to improve deep temperature match is suggested. Finally,
419 experimentation with other matrix fraction and porosity values in the rock could give best approach
420 and application of inverse modelling may be a tool to improve parameter selection since this study
421 used only the manual calibration and though the model can be recalibrated to get closer to more

422 realistic values, under its current conditions, it shows the potential to be used for shallow injection
423 management

424 **6. Conclusions**

425 Numerical models are a simplified way of representing reality and in this first attempt at matching
426 temperature and tracer data, it is unsurprising that there is some discrepancy in the model. This
427 modeling study focused solely on the recovery of the injection 2,7-NDS tracer that was injected
428 into well NN-6. The grid generation and model setup mainly focused on the geometry of the
429 shallow lava field and major faults, and the resolution is limited at deep levels. Unfortunately,
430 there is no data on the pressure at the deep levels, which makes it difficult to interpret and model
431 deeper injection. The model is sensitive to even but the slight changes in model configuration
432 parameters or structures.

433 The numerical model reproduces the increasing temperatures within the postglacial lava
434 flow in response to reinjection. The model shows an acceptable match for most monitoring stations
435 which reflected a representation of the temperature spread from 1998 to 2018. There are two main
436 permeable channels, and flow is largely confined within these permeable features found between
437 the Nesjavellir reinjection zone to Lake Thingvellir. The measured tracer recovery and peak for
438 the monitoring stations fits well with the simulations, but the tracer arrival time for natural outflows
439 could be improved.

440 The medium at deep levels appears to be strongly anisotropic, where extensive faults act
441 as a preferential pathway for the re-injected fluid. Through the fault zone, flow easily flows where
442 fractures interconnect with shallow permeable channels at shallow levels, allowing some of the

443 fluid to reach the surface layers. However, the area near the lake has complex technical
444 characteristics, being somewhat unclear as to the transport of flows in that area.

445 Given that the temperature and the tracer simulation match the field data with the selected
446 hydrological parameters, the model shows that it is possible to make a forecast on the possible
447 behavior of the system. With continuous injection, the temperature after 20 years will be around
448 35 °C for shallow levels (-90 masl.) and higher than 50 °C for intermediate and deeper levels below
449 lava flow limited with the Lake Thingvellir. In the event that the injection is interrupted and is not
450 resumed, the temperature will be close to initial condition shallow levels around all the lava flow
451 field, especially near Lake Thingvellir, after only a few years. However, the area around the
452 deepest injection zone it will take more than 20 years to cool down until be close to the steady
453 state temperature according to the model.

454 **Availability of data and materials**

455 The data that support the findings of this study are available from Reykjavik Energy (OR) but
456 restrictions apply to the availability of these data, which were used under license for the current
457 study, and so are not publicly available. Data are however available from the authors upon
458 reasonable request and with permission of Reykjavik Energy (OR).

459 **Acknowledgments**

460 The authors thank Reykjavik Energy (OR) for providing valuable data, assistance, and support
461 during this research. Due to the nature of this research, the policy and privacy of the entity that
462 owns the dataset, the supporting data is not available for sharing publicly.

Authors' contributions

EG-D constructed the 2D maps, 3D geologic model and set up the numerical model with the assistance of TR. EG-D conducted the calibration and simulations, and wrote the manuscript with the collaboration of SS. All authors participated in the interpretation of the numerical simulations and enhances to the numerical model and discussion of general results. SS and JN participated in a significant part in the revision of the manuscript and contributed to every aspect of the study. TR and SS supported in large part with improving the code script throughout the rsearch. All authors read and approved the final manuscript.

Competing interests

The authors declare that they have no known competing financial interests or personal relationships that could have appeared to influence the work reported in this paper

Funding

Open Access funding enabled and organized by Projekt DEAL. The research received no specific grant from any funding agency in the public, commercial, or not-for-profit sectors.

References

Arnason, B., Theodorsson, P., Bjornsson, S. and Saemundsson, K. Hengill, a high temperature area in Iceland. Bulletin of Volcanology. 1969; 33,245-160. doi.org/10.1007/BF02596720

Axelsson, G. Importance of geothermal reinjection. In Proceedings: Workshop for Decision Makers on the Direct Heating Use of Geothermal Resources in Asia, organized by UNU-GTP, TBLRREM and TBGMED, Tianjin, China, 2008;15 pp.

Axelsson, G. Role and management of geothermal reinjection. Short Course on Geothermal Development and Geothermal Wells", organized by UNU-GTP and LaGeo, Santa Tecla, El Salvador, 2012.

Axelsson, G. Tracer tests in geothermal resource management. EPJ Web of Conferences. 2013; 50:02001. doi: 10.1051/epjconf/20135002001.

Barenblatt, G.I., Zheltov, I.P., and Kochina, I.N. Basic concepts in the theory of seepage of homogeneous liquids infissured rocks. Journal of Applied Mathematics and Mechanics. 1960;245: 1286-1303. doi:10.1016/0021-892860)90107-6

Björnsson, G. Endurskoðað hugmyndalíkan af jarðhitakerfum í Hengli og einfalt mat á vinnslugetu nýrra borsvæða. Skýrsla 3 - 2007, Orkuveita Reykjavíkur – Nýjar virkjanir. 2007.

Björnsson, S., Gudmundsdottir, I.D., Ketilsson, J. Geothermal Development and Research in Iceland, Orkustofnun. 2010. https://nea.is/media/utgafa/GD_loka.pdf. Accessed 12 October 2021.

Bodvarsson, G.S., Bjornsson, S., Gunnarsson, A., Gunnlaugsson, E., Sigurdsson, O., Stefansson, V. and Steingrimsson, B. A. Summary of Modeling Studies of the Nesjavellir Geothermal Field, Iceland. In Proceedings: 13th Workshop on Geothermal Reservoir Engineering, Stanford University, CA, USA. 1988.

Bodvarsson, G.S., Bjornsson, S., Gunnarsson, A., Gunnlaugsson, E., Sigurdsson, O., Stefansson, V. and Steingrimsson, B. The Nesjavellir Geothermal Field, Iceland, Part I. Field Characteristics and Development of a Three-dimensional Numerical Model. Geothermal Science and Technology. 1990;23:189-228.

Bodvarsson, G.S., Bjornsson, S., Gunnarsson, A., Gunnlaugsson, E., Sigurdsson, O., Stefansson, V. and Steingrimsson, B. The Nesjavellir Geothermal Field, Iceland, 2. Evaluation of the Generating Capacity of the System. Geothermal Science and Technology. 1991;24:229-261.

Bodvarsson, G.S., Gislason, G., Gunnlaugsson, E., Sigurdsson, O., Stefansson, V., and Steingrimsson, B. Accuracy of Reservoir Predictions for the Nesjavellir Geothermal Field, Iceland. In Proceedings: 18th Workshop on Geothermal Reservoir Engineering, Stanford University, CA, USA, 1993.

Croucher, A. PyTOUGH: a Python scripting library for automating TOUGH2 simulations. In Proceedings: 33rd New Zealand Geothermal Workshop, Auckland, New Zealand, 2011.

Croucher, A. and O'Sullivan, M. J. Approaches to local grid refinement in TOUGH2 models. In Proceedings: 35th New Zealand Geothermal Workshop, Rotorua, New Zealand, 2013.

Franzson, H. Nesjavellir-Borholujarðfræði, vatnsgengd í jarðhitageymi. OS-88046/JHD-09. 1988; 58 p.

Franzson, H. Hydrothermal evolution of the Nesjavellir high-temperature system, Iceland. In Proceedings: World Geothermal Congress 2000, Kyushu-Tohoku, Japan, 2000.

Franzson, H., Kristjánsson, B.R., Gunnarsson, G., Björnsson, G., Hjartarson, A., Steingrímsson, B., Gunnlaugsson, E. and Gíslason, G. The HengillHellisheiði Geothermal Field. Development of a Conceptual Geothermal Model. In Proceedings: World Geothermal Congress, Antalya, Turkey, 2005.

Franzson, H., Gunnlaugsson, E., Árnason, K., Sæmundsson, K., Steingrímsson, B., and Harðarson, B.S. The Hengill Geothermal System, Conceptual Model and Thermal Evolution. In Proceedings: World Geothermal Congress 2010, Bali, Indonesia, 2010.

Gíslason, G. Nesjavellir co-generation plant, Iceland. Flow of geothermal steam and noncondensable gases. In Proceedings: World Geothermal Congress 2000, Kyushu-Tohoku, Japan, 2000.

Gunnarsson, G. and Aradóttir E.S. The Deep Roots of Geothermal Systems in Volcanic Areas: Boundary Conditions and Heat Sources in Reservoir Modeling. Transport in Porous Media. 2014; 1081:43–59. doi.org/10.1007/s11242-014-0328-1

Gunnarsson, A., Steingrimsson, B., Gunnlaugsson, E., Magnusson, J., and Maack, R. Nesjavellir Geothermal Co-generation Power Plant. Geothermics. 1992;21:559-583. doi.org/10.1016/0375-6505(92)90007-V

Gunnarsson, G., Arnaldsson, A. and Oddsdóttir, A.L. Model Simulations of the Hengill Area, Southwestern Iceland. Transport in Porous Media. 2011;90:3-22. doi.org/10.1007/s11242-010-9629-1.

Hafstað, Þ.H., Vilmundardóttir E.G. and Kristjánsson B.R. Nesjavellir. Rannsóknarborholur í hraununum á affallssvæði virkjunarinnar. Iceland GeoSurvey, ÍSOR-2007/058. 2007; 65 p.

Pruess, K. GMINC: A Mesh Generator for Flow Simulations in Fractured Reservoirs: Lawrence Berkeley Laboratory Report LBL-15227. Berkeley, California. 1983.

Pruess, K. and Narasimhan, N.T. A Practical Method for Modeling Fluid and Heat Flow in Fractured Porous Media. Society of Petroleum Engineers Journal. 1985;251:14-26. doi.org/10.2118/10509-PA

Pruess, K. Brief Guide to the MINC - Method for Modeling Flow and Transport in Fractured Media. Earth Sciences Division, Lawrence Berkeley National Laboratory. Berkeley, CA, USA. LBL-32195. 1992.

Ratouis, T. M., Snæbjörnsdóttir, S. O., Gunnarsson, G., Gunnarsson, I., Kristjánsson, B. R., and Aradóttir, E. S. Modelling the Complex Structural Features Controlling Fluid Flow at the CarbFix2 Reinjection Site, Hellisheiði Geothermal Power Plant, SW-Iceland. In Proceeding: 44th Workshop on Geothermal Reservoir Engineering, Stanford University, CA, USA, 2019.

Shook, M.G. A Systematic Method for Tracer Test Analysis: An Example Using Beowawe Tracer Data. In Proceedings, 30th Workshop on Geothermal Reservoir Engineering, Stanford University, CA, USA, 2005.

Shook, M.J., and Forsmann, H.J. Tracer Interpretation Using Temporal Moments on a Spreadsheet, Idaho National Laboratory Report, INL/EXT-05-00400. 2005. https://inldigitallibrary.inl.gov/sites/sti/sti/3028333.pdf. Accessed 12 October 2021.

Snæbjörnsdóttir, S., Wiese, F., Fridriksson, T., Ármansson, H., Einarsson, G. M., Gislason, S. R. CO2 storage potential of basaltic rocks in Iceland and the oceanic Ridges. Energy Procedia. 2014; 63:4585-4600. doi.org/10.1016/j.egypro.2014.11.491

Stevenson, J.A., Mitchell, N.C., Mochrie, F., Cassidy, M., Pinkerton, H. Lava penetrating water: the different behaviours of pahoehoe and ‘a‘a at the Nesjahraun, Þingvellir, Iceland. Bulletin of Volcanology. 2012;74:33–46. doi10.1007/s00445-011-0480-1

Wagner, W., and Pruß, A. The IAPWS Formulation 1995 for the Thermodynamic Properties of Ordinary Water Substance for General and Scientific Use. The Journal of Physical Chemistry. Reference Data. 2002;312:387-535. doi.org/10.1063/1.1461829

Warren, J.E., and Root, P.J. The behavior of naturally fractured reservoirs. Society of Petroleum Engineers Journal. 1963;33:245–255. doi.org/10.2118/426-PA

599 Yeh, A., Croucher, A. and O'Sullivan, M.J. Recent developments in the AUTOUGH2 simulator.
600 In Proceedings: TOUGH Symposium, Berkeley, California, 2012.
601
602 Yeh, A., Croucher, A. E., and O'Sullivan, M.J. TIM–Yet another Graphical Tool For TOUGH2.
603 In Proceeding: 35th New Zealand Geothermal Workshop, Rotorua, New Zealand, 2013.
604
605 Zakharova, O.K., and Spichak, V.V. Geothermal fields of Hengill Volcano, Iceland.
606 Journal of Volcanology and Seismology. 2012;6:1–14. doi.org/10.1134/S074204631201006X

Figures

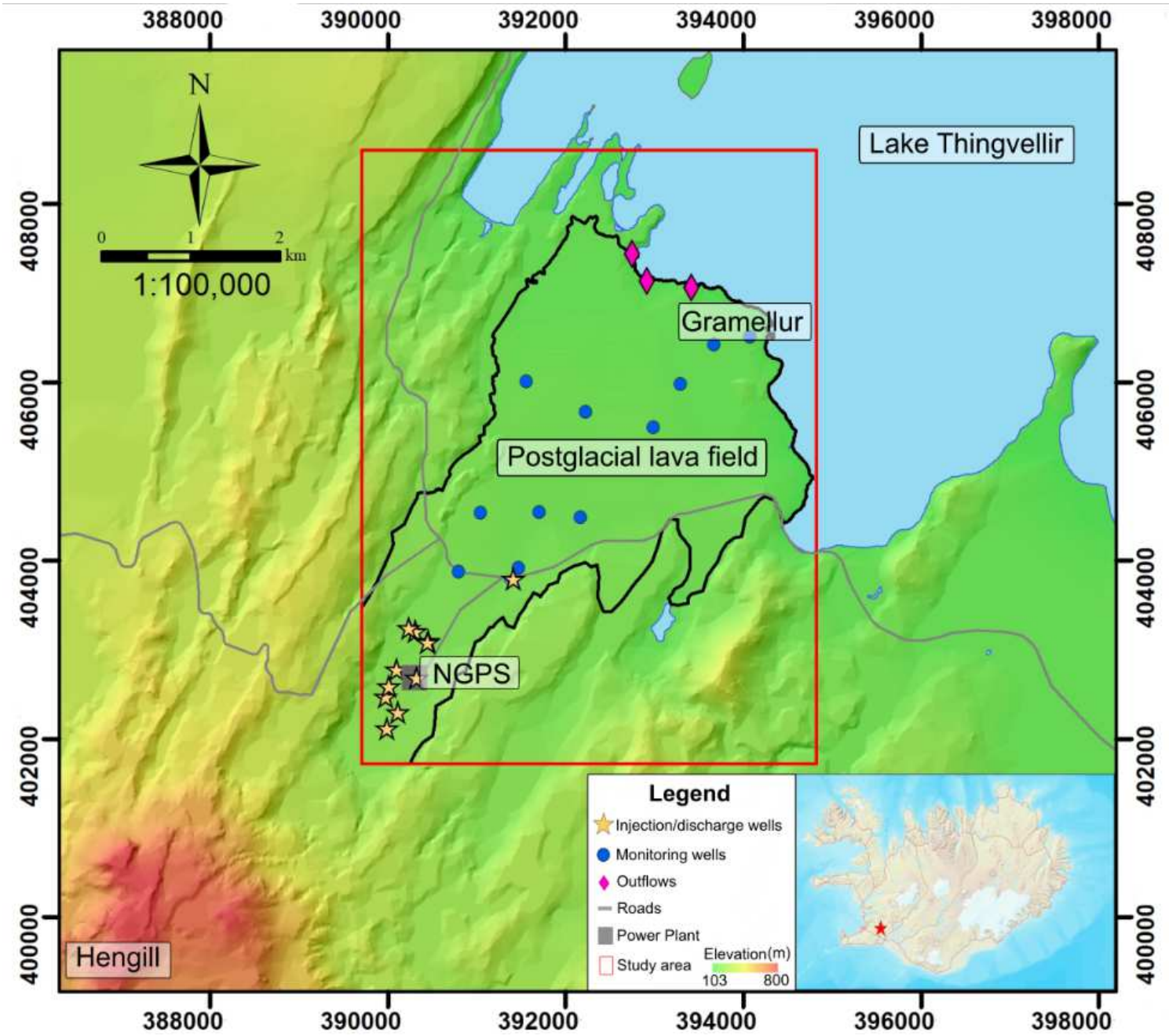

Figure 1

Location of Nesjavellir geothermal field. Red box is the study zone, and the main area of interest is within the black border line. NGPS: Nesjavellir Geothermal Power Station.

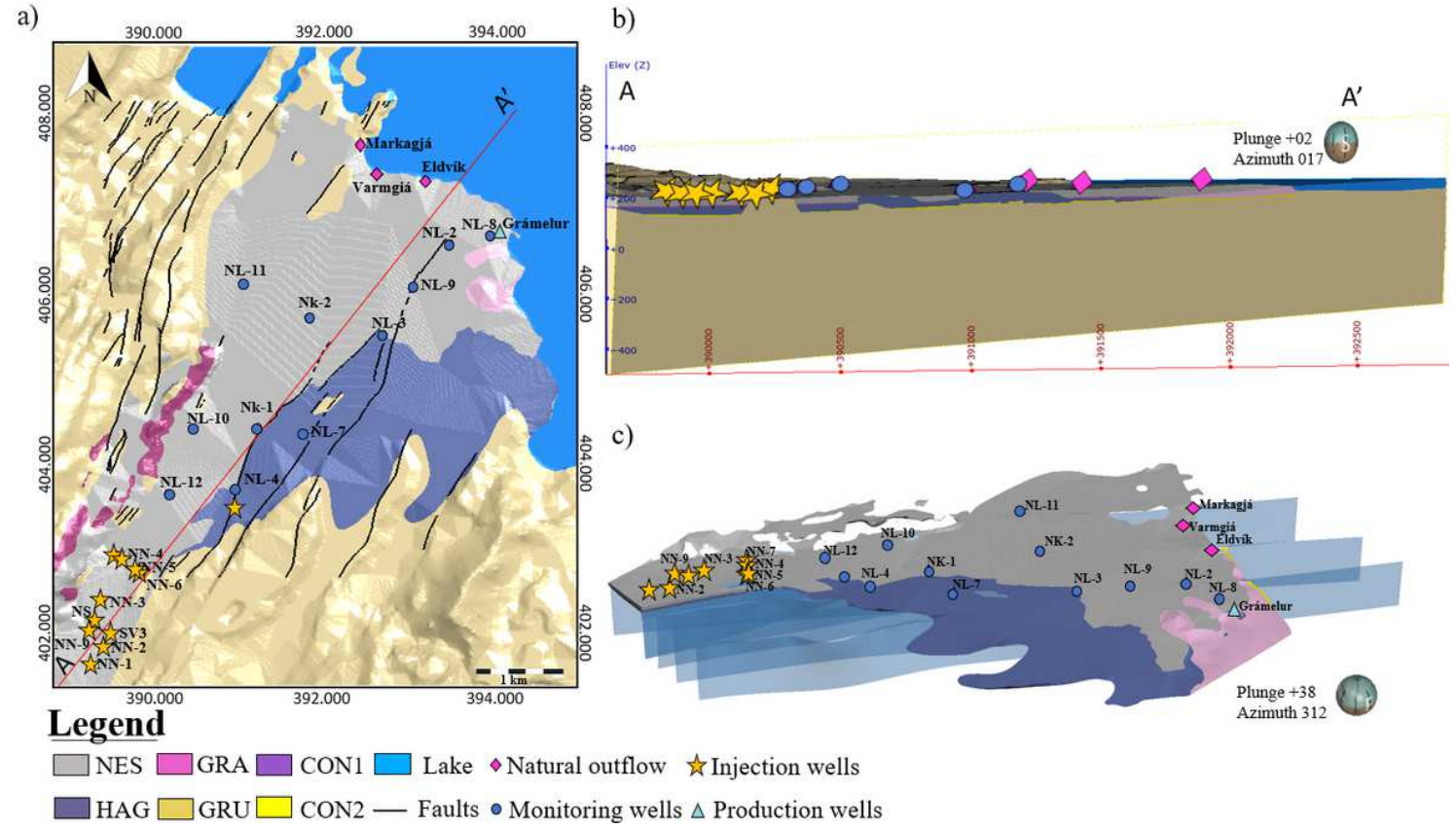

Figure 2

Nesjavellir geothermal system. a) Geological map of the survey area, after Hafstað et al. (2007). b) Cross-section A-A' showing major stratigraphic units, Nesjahraun lava flow (NES), Hagavíkurhraun lava flow (HAG), Grámelur cone fragments (GRA) and Grunnberg composite hyaloclastite and lavas (GRU). c) Detailed view of lava flows and fault planes.

Figure 3

a) 3-D geological model with fault planes projection. b) Cross-section showing the feedzones in blue spheres and injection wells in black NN-1, NN-02, NN-03, NN-04, NN-05, NN-06, NN-07, NN-09.

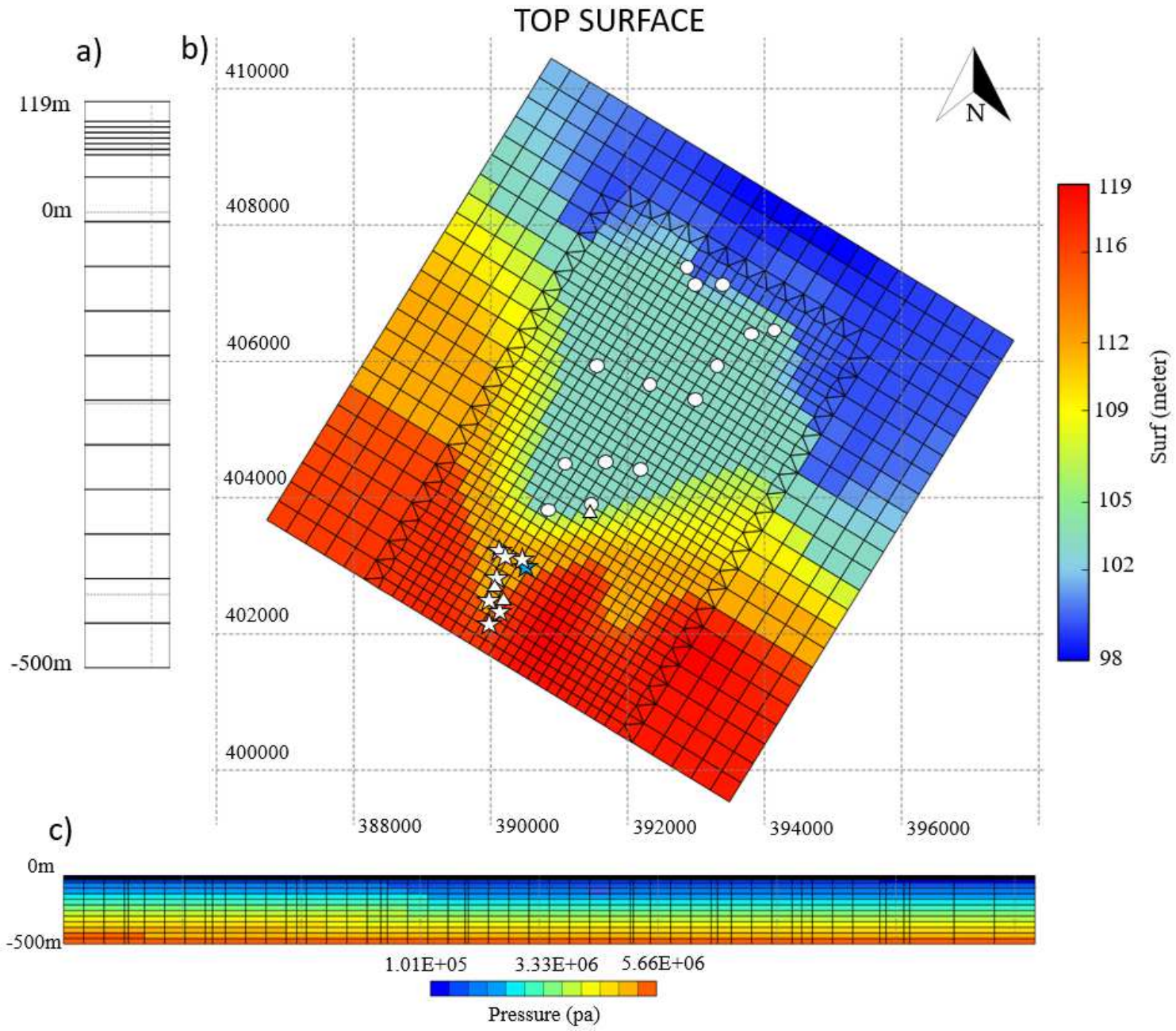

Figure 4

Grid refined and optimized with PyTOUGH visualized in TIM. (a) Layer structure of the model. (b) Top surface elevation. (c) Cross section with values of the initial pressure. White points are monitoring recovery stations and white stars are the injection wells.

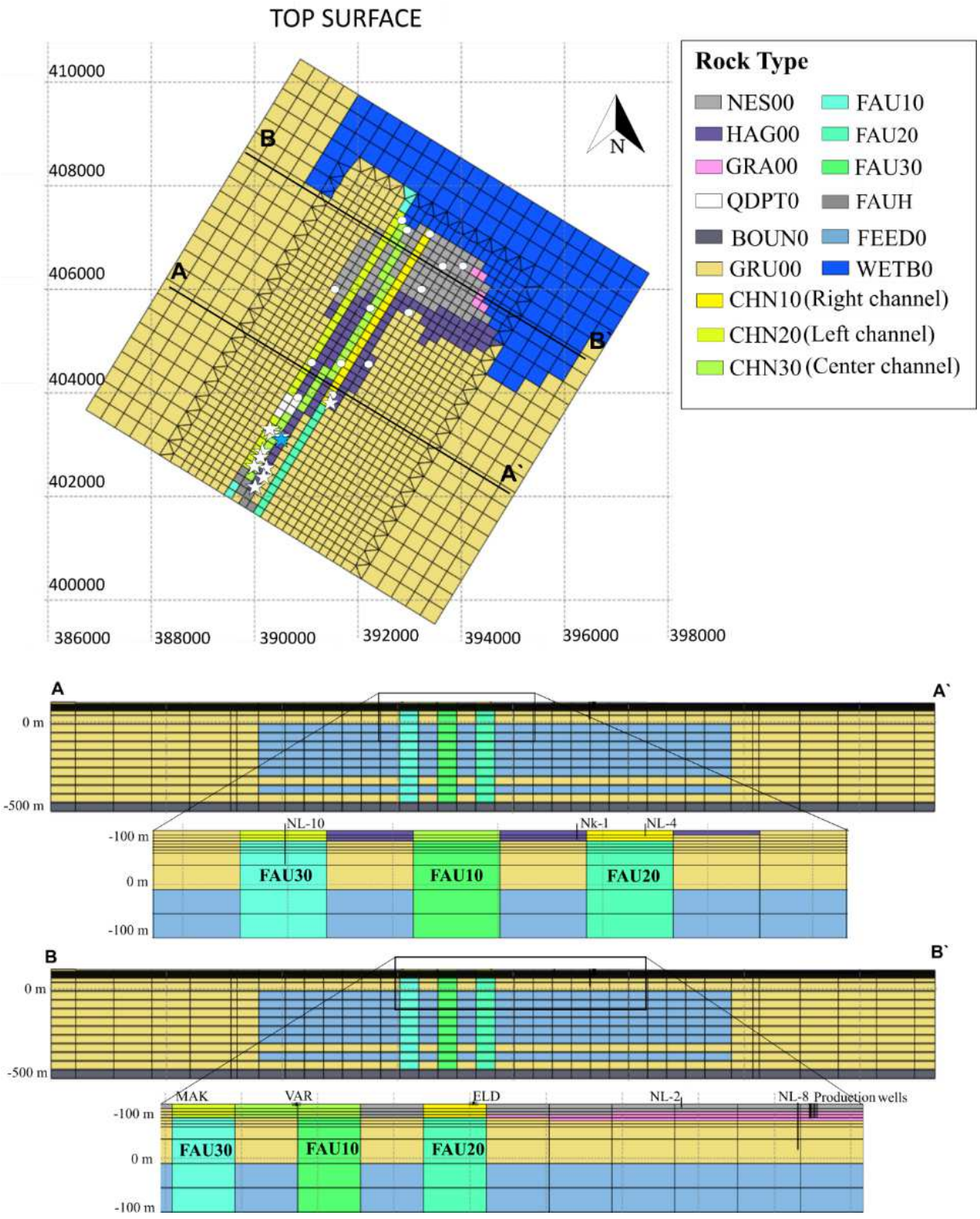

Figure 5

Calibrated model structure. White stars show injection wells, blue star NN-6 injection well and white points monitoring points. The NS transverse faults represented by FAU 10, FAU 20 and FAU 30.

Figure 6

Tracer test performed in 2018-2019. Injection of 2,7-NDS tracer injected in NN-6 (blue star). Map illustrates the trajectory and measured recovery times of 2,7-NDS between injection and monitoring stations.

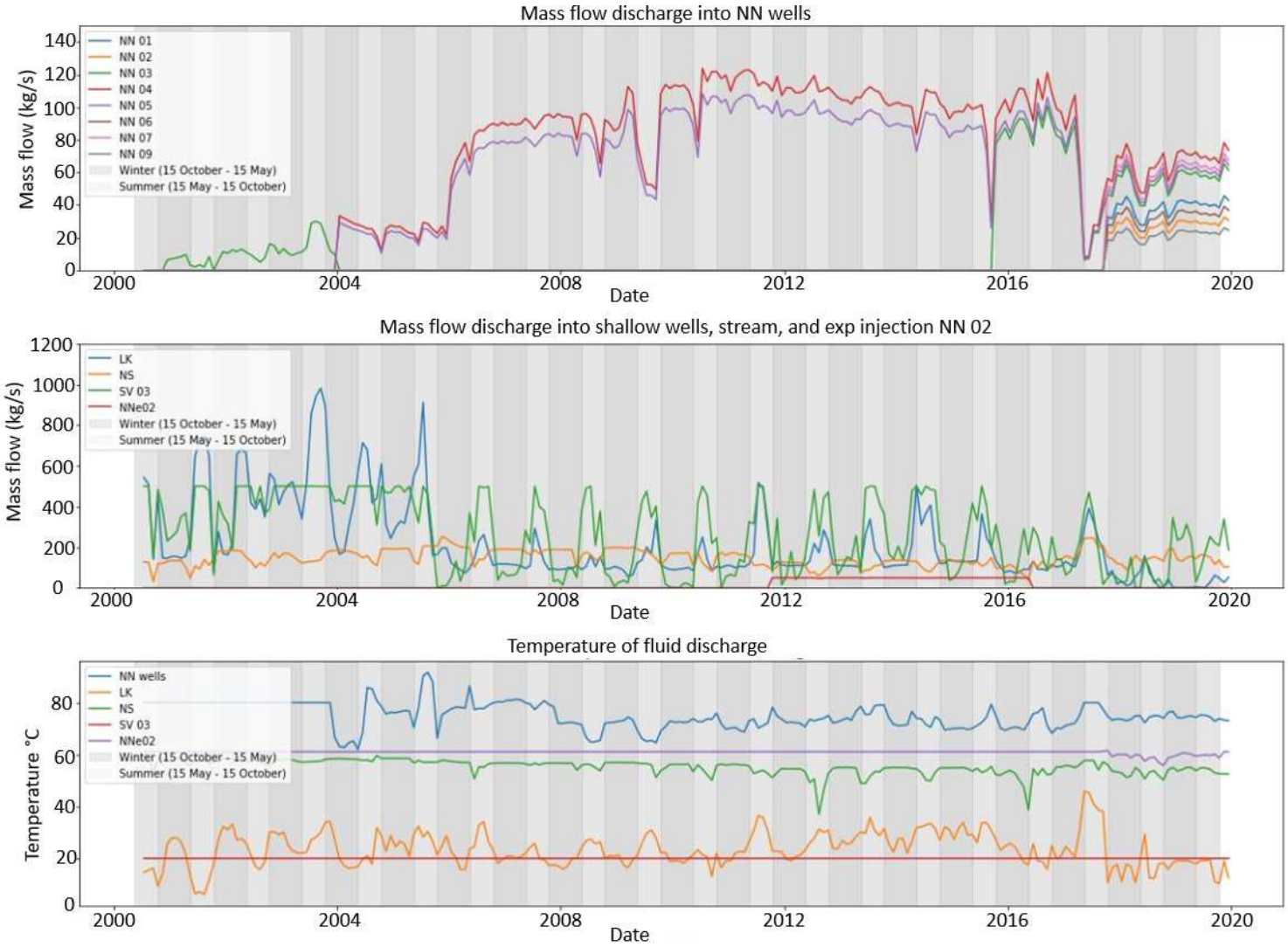

Figure 7

Total injection rates and temperature of injected water during the simulation time. Dark shades of grey are the winter season and light shades are summer season.

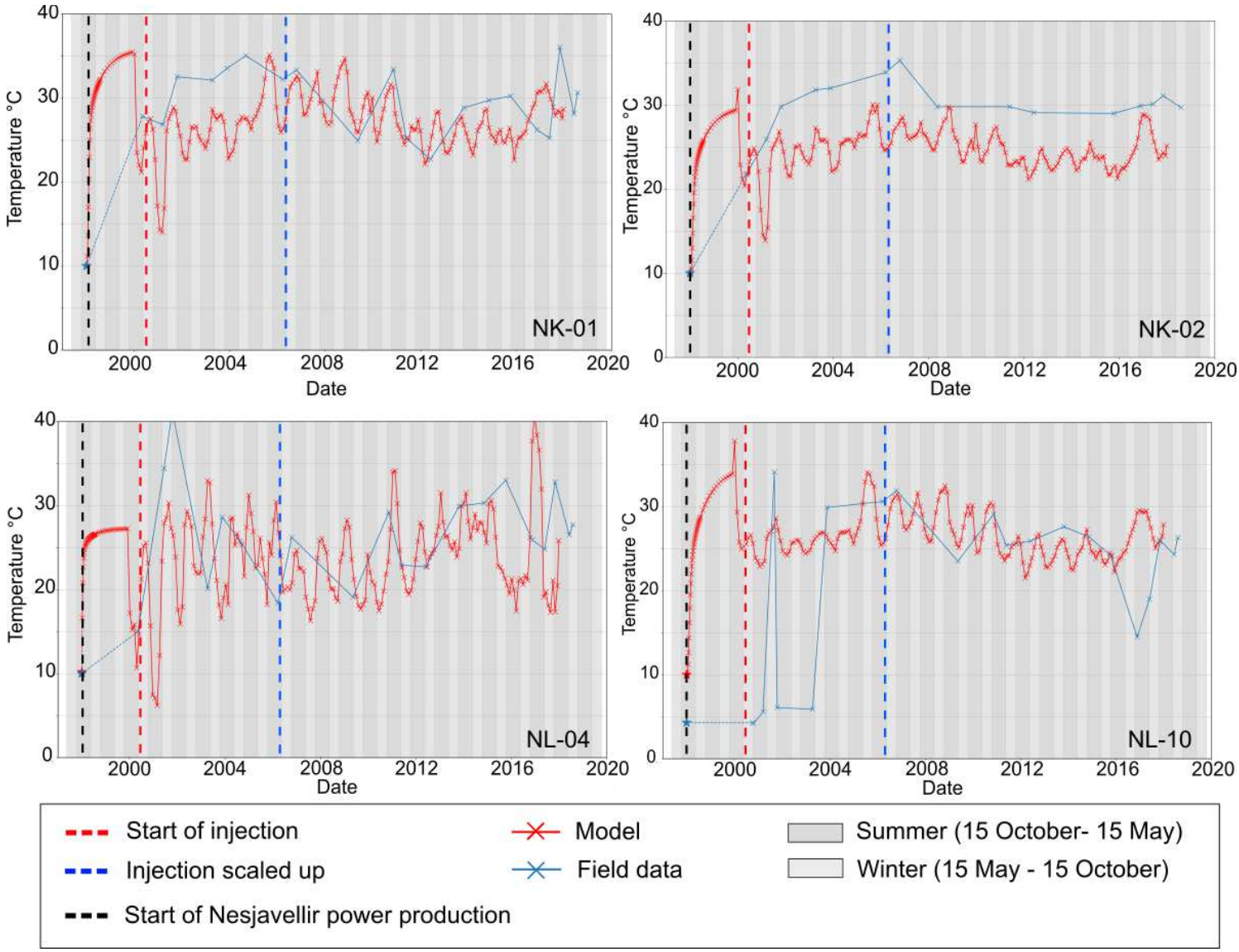

Figure 8

Evolution of temperature from 1998 to 2018 at one meter of groundwater level layer 1) in NK-01, NK-02, NL-04 and NL-10. Field data in blue and model results in red.

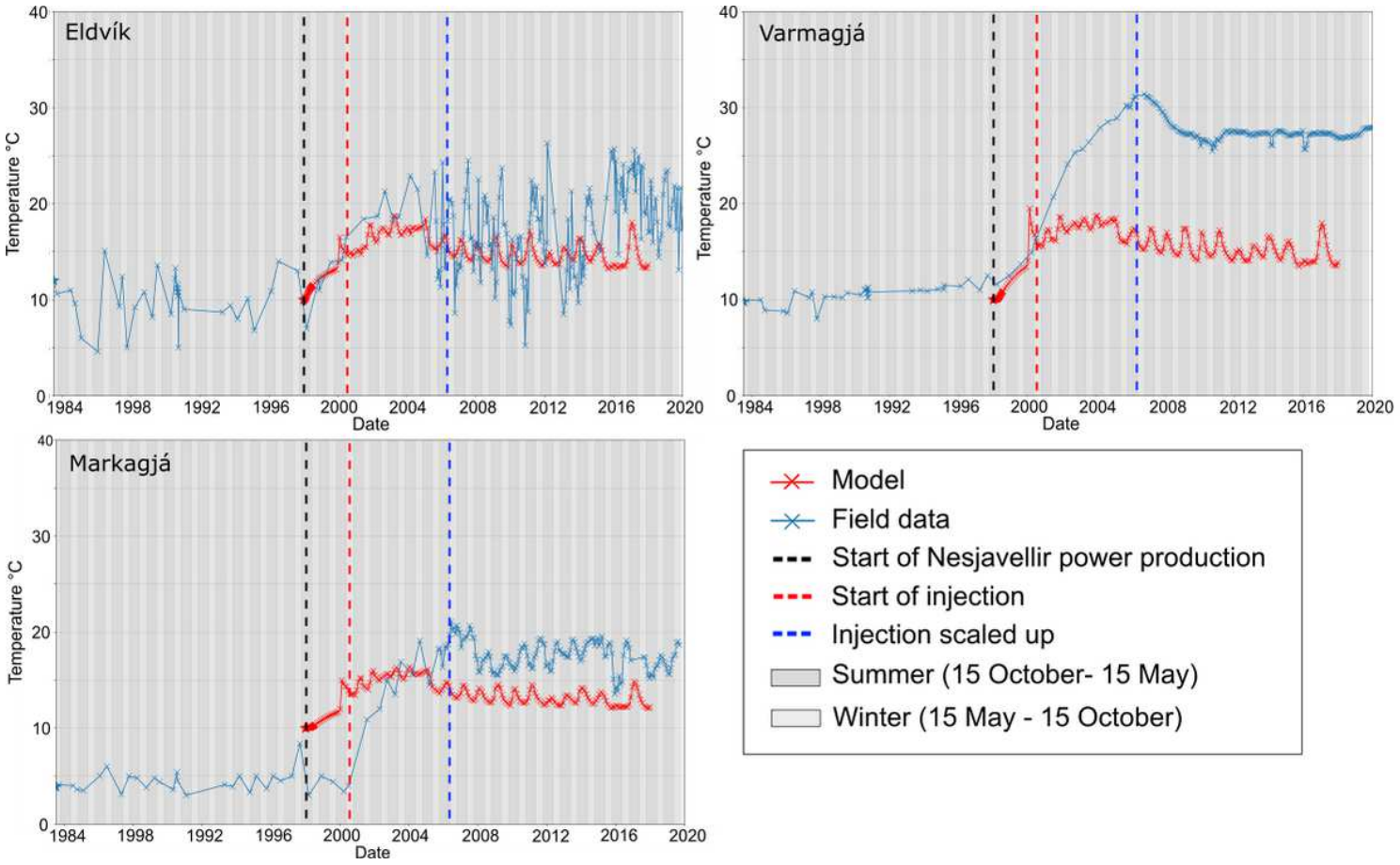

Figure 9

Evolution of temperature from 1998 to 2018 for springs at 100 masl. (Layer 1). Field data in blue and model results in red.

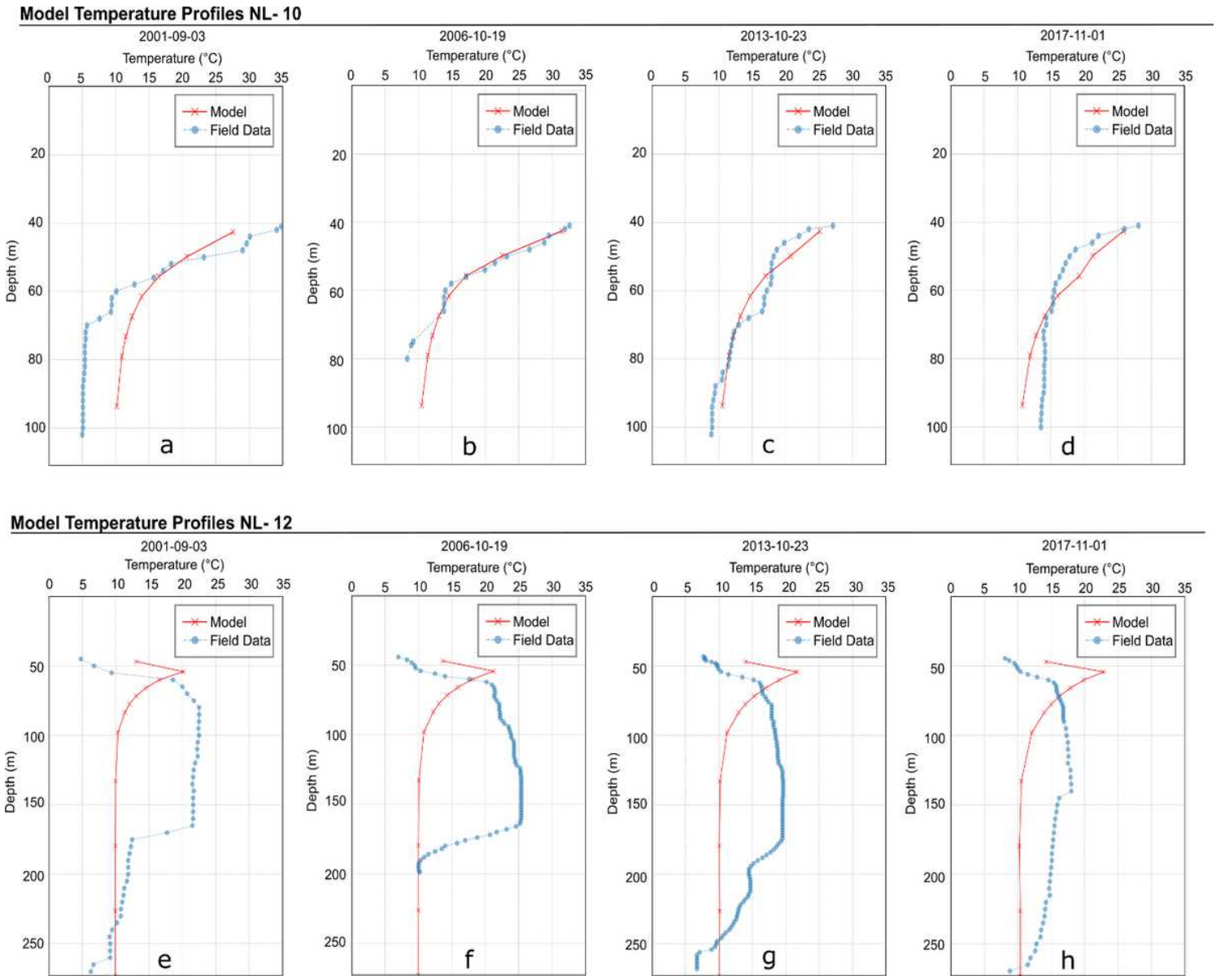

Figure 10

Comparison between modeled (red lines) and measured (blue lines) temperature-depth profiles in NL-10 (a-d) and NL-12 (e-h). Figure shows results on 2001-09-03(a,e), 2006-10-19(b,f), 2013-10-23(c,g), and 2017-11-01(d, h).

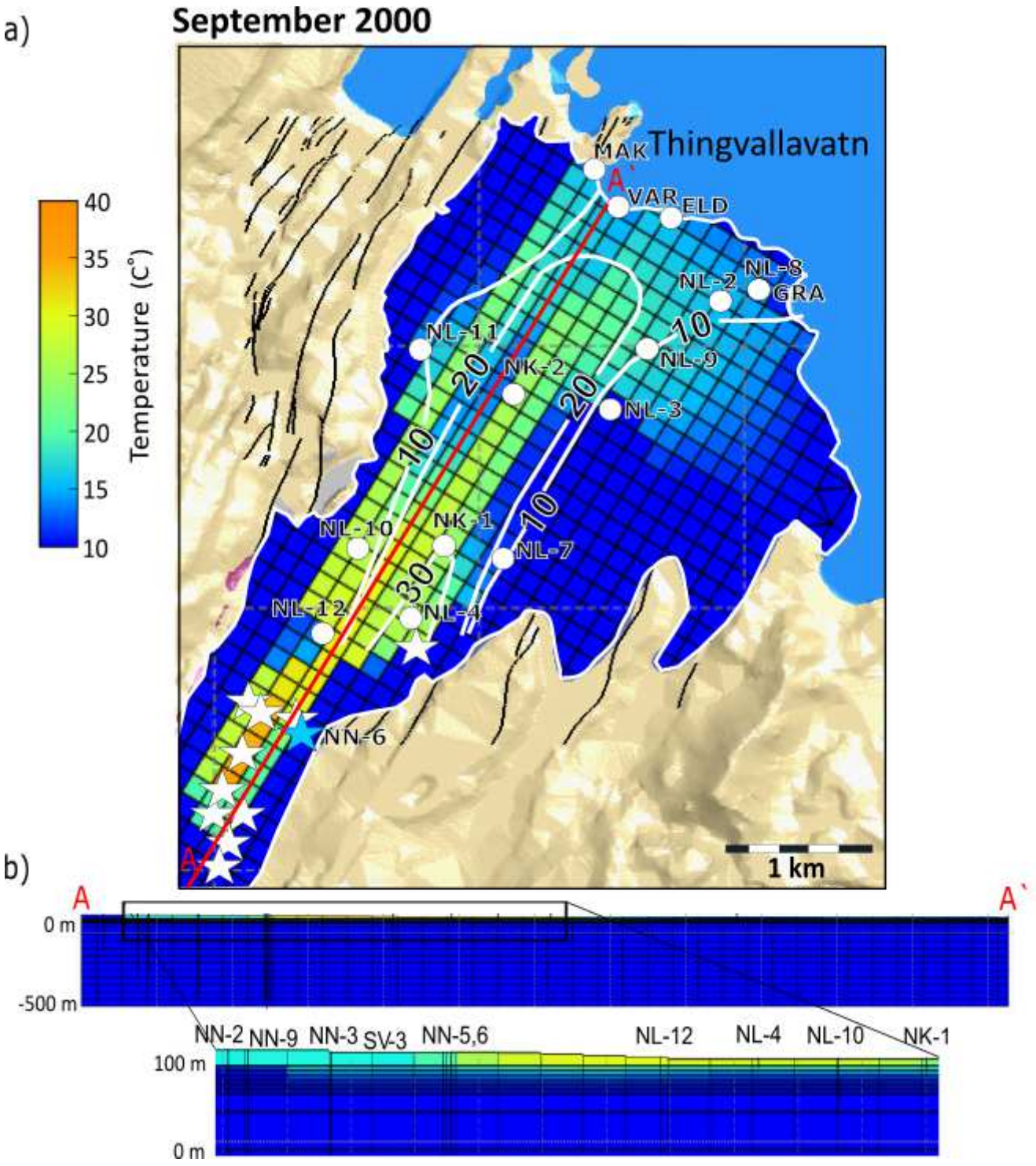

Figure 11

a) Comparison between measured temperature at one meter the below groundwater table for September 2000. The contours lines represent the temperature registered from ISOR data. White dots are the monitoring station, white stars are the injection wells and blue star is the injection well NN-6 chosen for the tracer test. b) Cross section along the most permeable fault (FAU10).

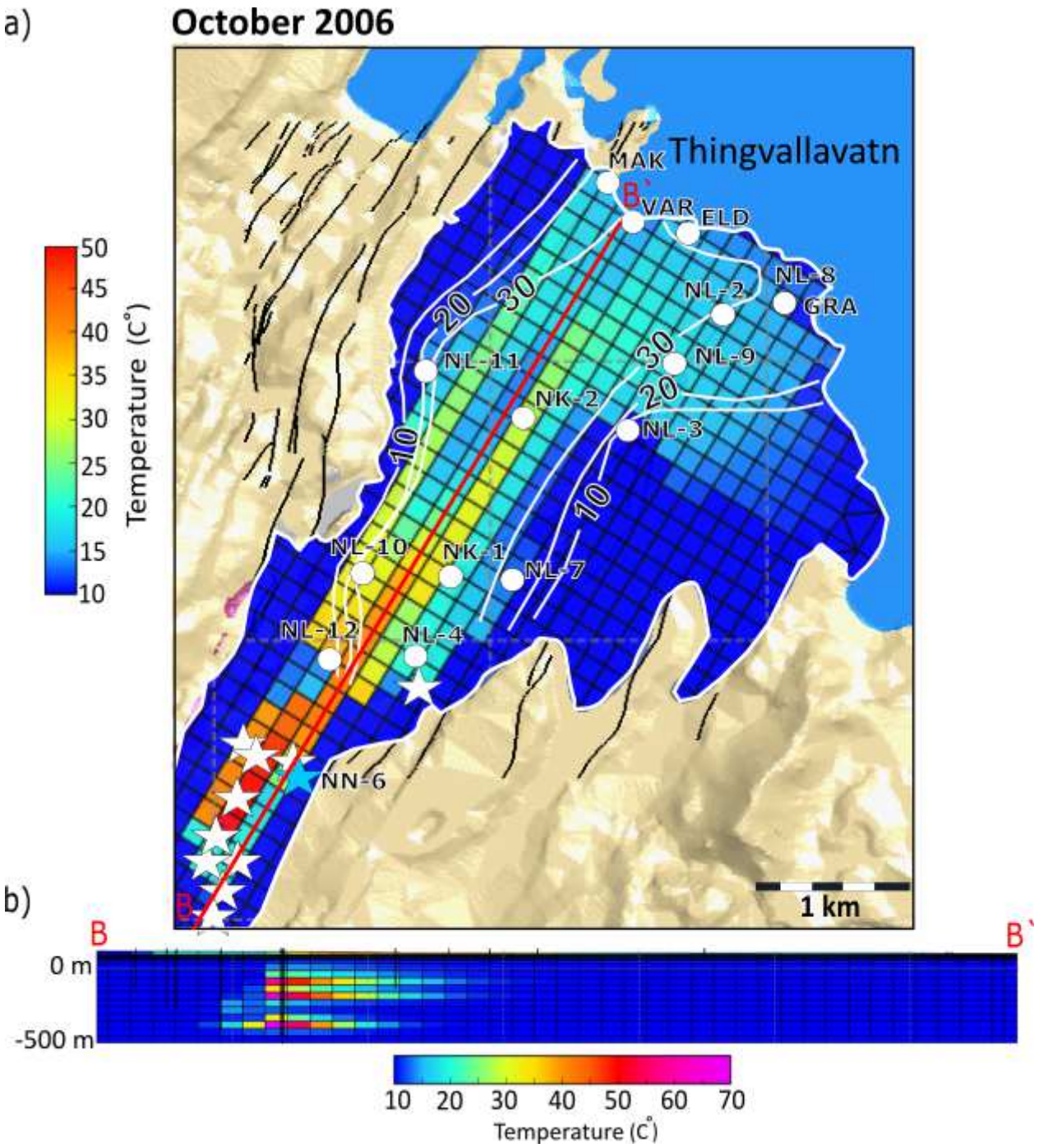

Figure 12

a) Comparison between temperature ISOR map and simulation for October 2006. White dots are the monitoring station, white stars are the injection wells and blue star is the injection well NN-6 chosen for the tracer test. Groundwater temperature one meter below the groundwater table. b) Cross section along the most permeable fault (FAU10).

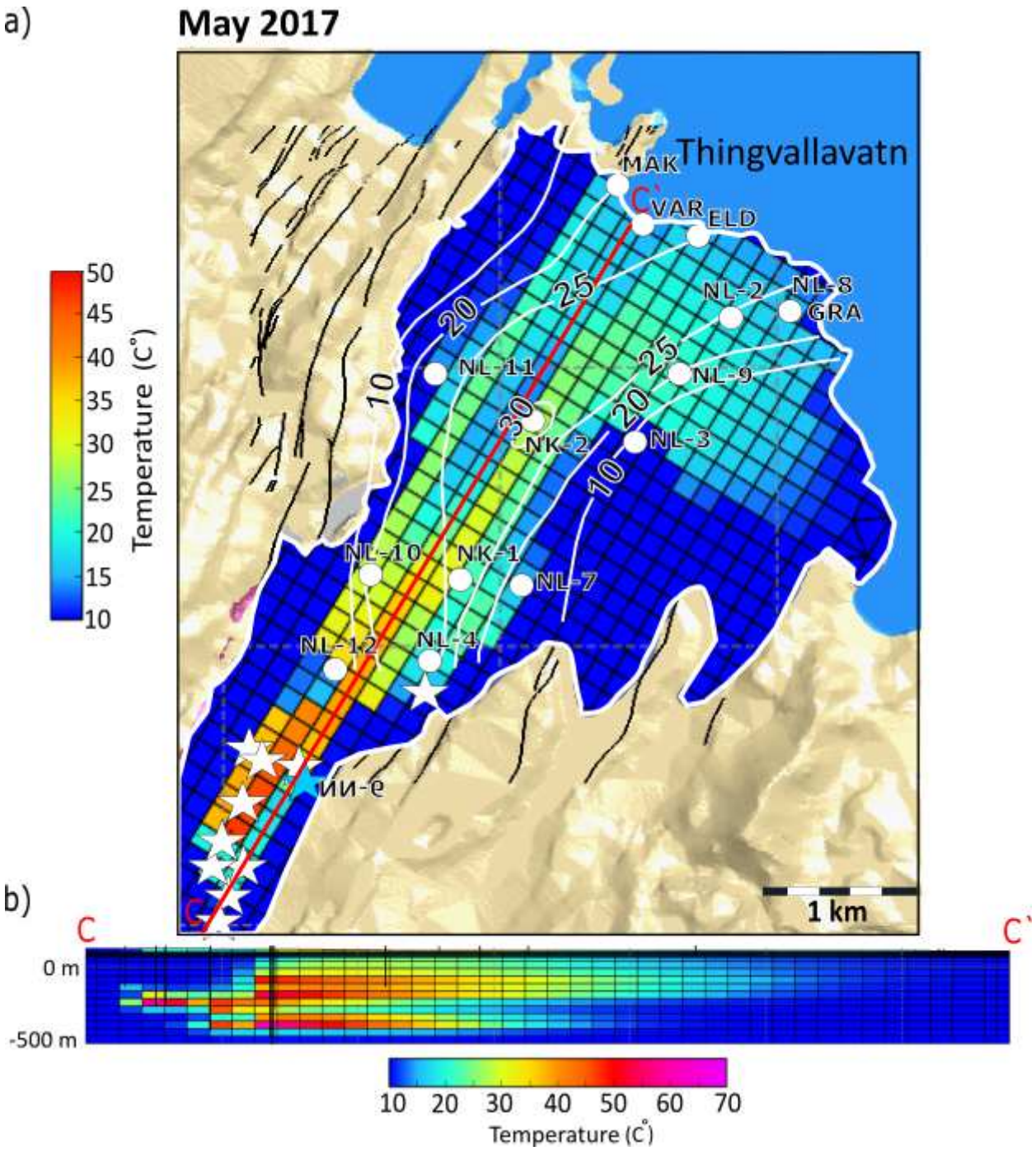

Figure 13

a) Comparison between temperature ISOR map and simulation for May 2017. White dots are the monitoring station, white stars are the injection wells and blue star is the injection well NN-6 chosen for the tracer test. Groundwater temperature one meter below the groundwater table. b) Cross section along the most permeable fault (FAU10).

Figure 14

Temperature model for 2018-2019 with comparison between Leapfrog temperature model and the simulation generated with AUTOUGH2. a) Map of temperature from 1998 to 2018 at one meter of groundwater level (layer 1). b) 3-D model comparison sections; Left Leapfrog model and right Simulation results.

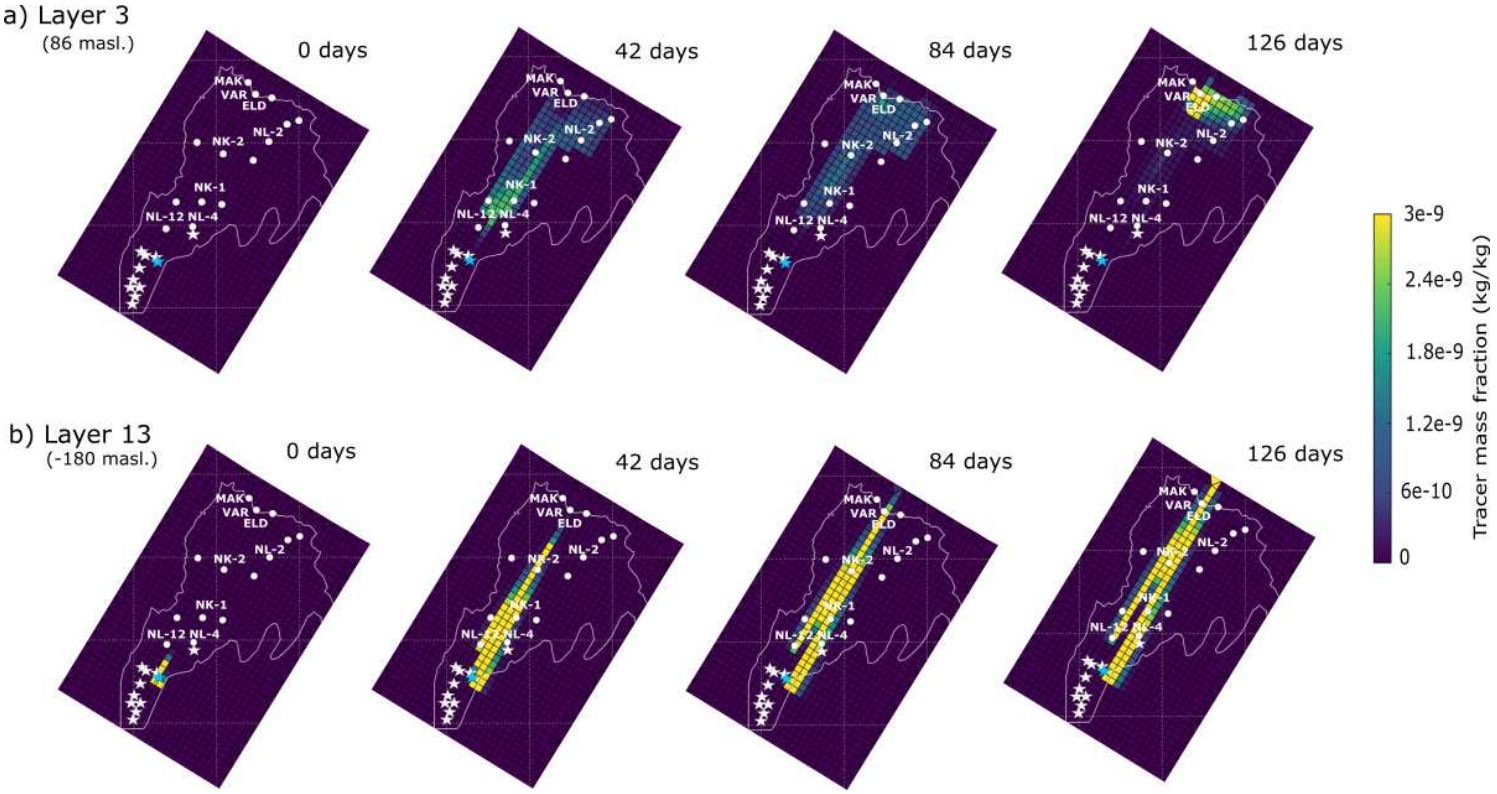

Figure 15

Dual-porosity model from 2018 to 2019. The results are shown at a different time intervals of 0 day, 42 days, 84 days and 126 days for layer 3 (a) and layer 13 (b).

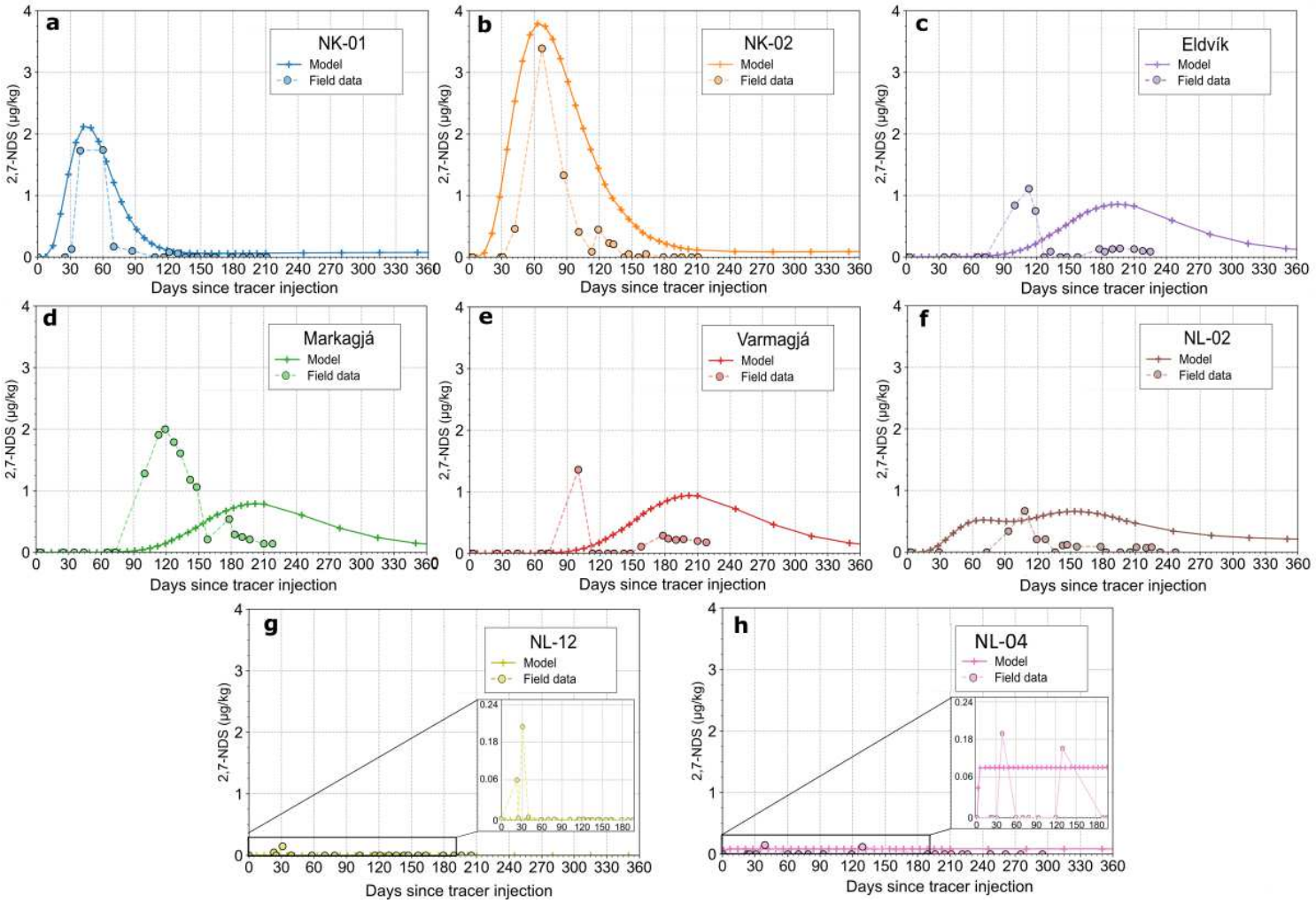

Figure 16

Dual-porosity model from 2018 to 2019- Tracer recovery curves for 2,7-NDS tracer injection (µg/kg). The field data is represented by the dots and the dotted line, and the model results by the plus sign symbol and the solid line

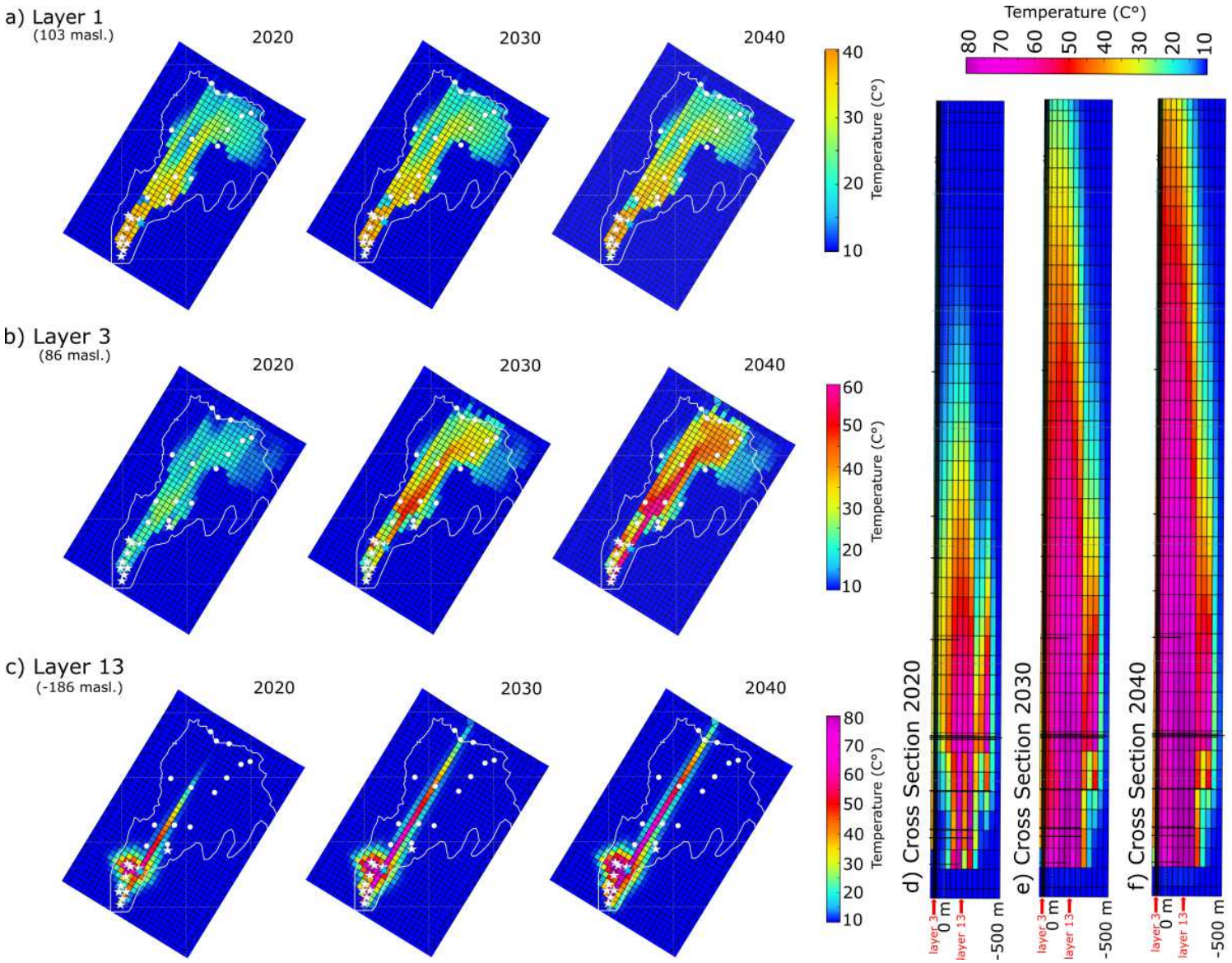

Figure 17

Evolution of temperature in 2020, 2030 and 2040 if injection and production continue at the same average flow rate and temperature from 2018 – 2020 overserved in layer 1 (a), layer 3 (b) and layer 13 (c). Cross section along the most permeable fault (FAU10) for 2020 (d), 2030 (e) and 2040 (f).

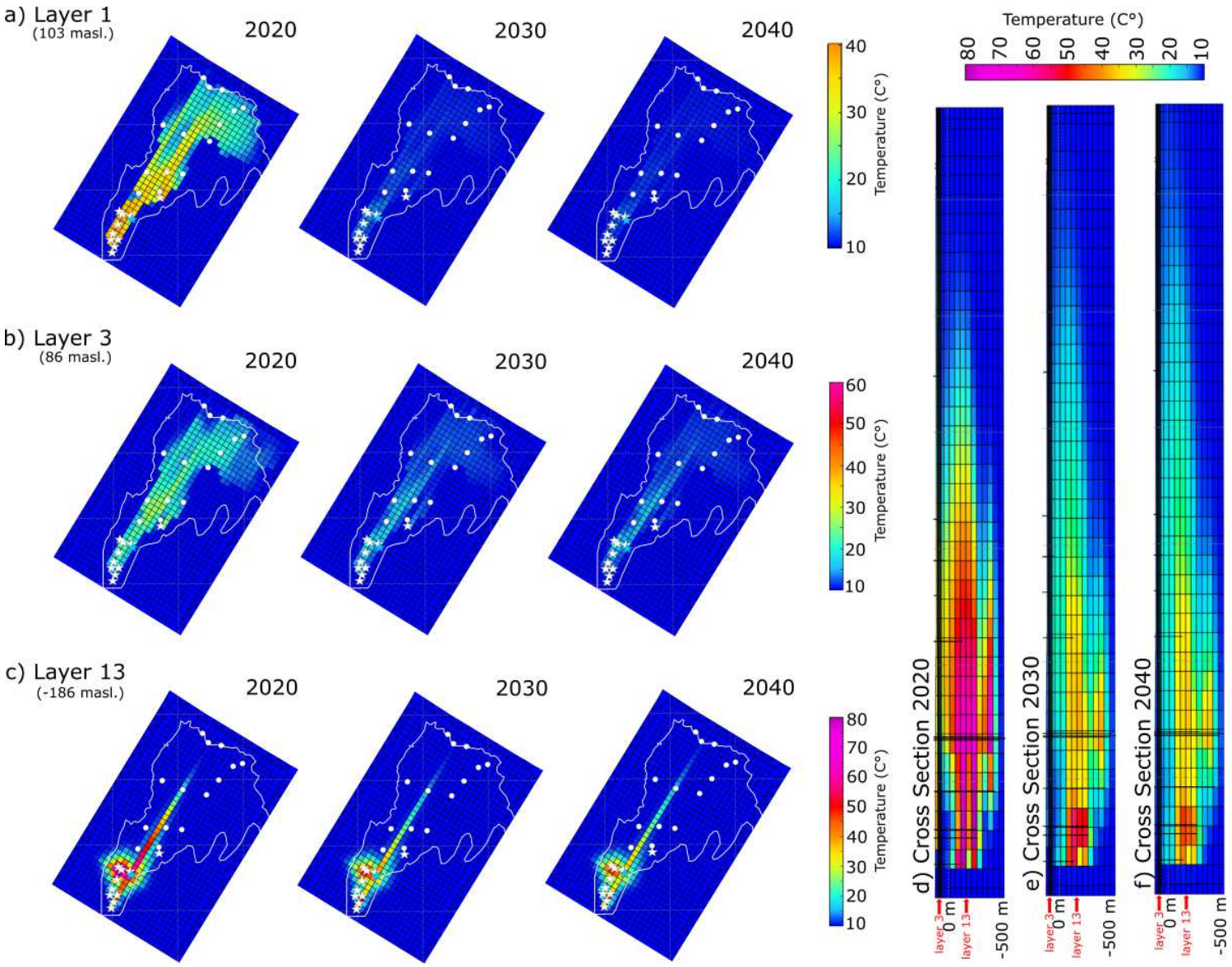

Figure 18

Evolution of temperature for 2020, 2030 and 2040 if all injection and production is stopped overserved in layer 1 (a), layer 3 (b) and layer 13 (c). Cross section shows temperature distribution along the most permeable fault (FAU10) for 2020 (d¬), 2030 (e) and 2040 (f).